Existence, Stability and Dynamics of Discrete Solitary Waves in a Binary Waveguide Array

Y. Shen,[1] P.G. Kevrekidis,[2,3] G. Srinivasan,[4] and A. B. Aceves[1]

[1]*Department of Mathematics, Southern Methodist University, Dallas, Texas 75275, USA*
[2]*Department of Mathematics and Statistics, University of Massachusetts, Amherst, Massachusetts 01003-4515 USA*
[3]*Center for Nonlinear Studies and Theoretical Division, Los Alamos National Laboratory, Los Alamos, NM 87544*
[4]*Theoretical Division, Los Alamos National Laboratory, Los Alamos, NM 87544*

arXiv:1510.08426v1 [physics.optics] 28 Oct 2015

Recent work has explored binary waveguide arrays in the long-wavelength, near-continuum limit, here we examine the *opposite* limit, namely the vicinity of the so-called anti-continuum limit. We provide a systematic discussion of states involving one, two and three excited waveguides, and provide comparisons that illustrate how the stability of these states differ from the *monoatomic* limit of a single type of waveguide. We do so by developing a general theory which systematically tracks down the key eigenvalues of the linearized system. When we find the states to be unstable, we explore their dynamical evolution through direct numerical simulations. The latter typically illustrate, for the parameter values considered herein, the persistence of localized dynamics and the emergence for the duration of our simulations of robust quasi-periodic states for two excited sites. As the number of excited nodes increase, the unstable dynamics feature less regular oscillations of the solution's amplitude.

I. INTRODUCTION

Over the past two and a half decades, the study of localized modes in nonlinear lattice dynamical systems has been a multi-faceted theme of research, that has now been summarized in numerous reviews [1]. Relevant applications span a wide number of disciplines and themes including, but not limited to, arrays of nonlinear-optical waveguides [2], Bose-Einstein condensates (BECs) in periodic potentials [3], micromechanical cantilever arrays [4], as well as Josephson-junction ladders [5], halide-bridged transition metal complexes [6], layered antiferromagnetic crystals [7], dynamical models of the DNA double strand [8], or granular crystals of beads interacting through Hertzian contacts [9].

Arguably, one of the most prototypical settings where such nonlinear states have emerged is that of optical waveguide arrays, where several of the relevant ideas and developments were first observed and analyzed, as has been summarized in for example [2, 10]. In fact, in this setting and the related context of photorefractive crystals, notions such as discrete diffraction [11] and its management [12], Talbot revivals [13], $\mathcal{PT}$-symmetry and its breaking [14], as well as discrete solitons [11, 15] and vortices [16, 17] have been experimentally observed. Another source of considerable inspiration has been the dynamics of Bose-Einstein condensates (BECs) in optical lattices [3, 18]. Yet, an additional motivation that has rendered such settings popular has been the existence of a prototypical (and deceptively simple) mathematical model that contains the main physical ingredients of diffraction and nonlinearity. This model is the well-known discrete nonlinear Schrödinger equation (DNLS) [19].

More recently, a number of variants of this theme of optical waveguide arrays have been studied in detail, notable examples being multi-component models involving multiple polarizations [20, 21], waveguides featuring quadratic (so-called χ^2) nonlinearities [22, 23], the examination of dark-solitonic states [24, 25] and the study of binary waveguide arrays [26–28]. Here, we focus more specifically on the theme of binary waveguide arrays and their alternating coupling structure.

In this study, we adopt the prototypical model of [26, 28], derived on the basis of coupled mode theory and incorporating the effects of distinct propagation constants on the two *components*, i.e., the even and odd waveguides. In earlier work [26, 28], emphasis was placed on quasi-continuum, long wavelength limits of the system. The discussion in those studies also included the potential for bearing band-gap and gap solitary waves, for supporting dark-bright solitary waves and strongly localized solutions, as well as a modulational instability (discrete and continuous) of the system. Here, our principal focus is on the highly localized solutions in the vicinity of the so-called anti-continuum (AC) limit [29]. In the neighborhood of the uncoupled limit between adjacent sites, following the approach of [30] but for this considerably more complex problem, we obtain a systematic set of results about the states that persist for finite coupling between the adjacent sites. We also explore the stability of the different configurations, developing a linear stability analysis and characterizing the dominant eigenvalues therein. We find that as the coupling varies between the two sets of waveguides, away from the monoatomic limit (of a single type of waveguides), the linearization eigenvalues may drastically change (e.g., real ones may become imaginary etc.). Finally, for the unstable configurations, that include populating up to four separate waveguides, we examine the dynamics for case examples we think are prototypical and for which we observe the formation of robust, quasi-periodic waveforms.

Our presentation is structured as follows. In section II, we briefly discuss the relevant physical model and associated properties/parameters thereof. Section III considers the existence of solutions near the AC limit. In section IV, the more complicated issue of the stability of the solutions is analyzed. Section V presents systematic computations for configurations of different types, populating 2-4 waveguides. Finally, in section VI, we summarize briefly our findings, and present our conclusions, as well as a number of directions for future work.

II. PHYSICAL MODEL AND SETUP

Following the earlier formulation of the binary waveguide model, on the basis of coupled mode theory (CMT) with Kerr nonlinearity [26, 28], the dynamical equations of interest read:

$$\begin{array}{l} iA_n{}' + \frac{\Delta\beta}{2}A_n + \varepsilon(C_1B_n + B_{n+1}) + \gamma_a|A_n|^2A_n = 0 \\ iB_n{}' - \frac{\Delta\beta}{2}B_n + \varepsilon(A_{n-1} + C_1A_n) + \gamma_b|B_n|^2B_n = 0 \end{array} \tag{1}$$

where $'$ denote $\frac{d}{dz}$. Here A_n and B_n denote the "even" and "odd" waveguides, and C_1 denotes the unequal coupling of the n-th waveguide with $n-1$ and $n+1$. We also introduce the parameter ε to control the strength of the coupling. $\Delta\beta$ denotes a detuning parameter, while $\gamma_{a,b}$ the nonlinear prefactors, are associated with the strength of the Kerr effect in the system. In the limit of $\varepsilon \to \infty$, for $C_1 = -1$ or $C_1 = 1$ (in respective vicinities of the Brillouin zone), one can devise a long wavelength limit of the system; for $C_1 = 1$ and $\Delta\beta = 0$, we fall back on the DNLS limit of waveguides of the same type. The key limit that we will utilize herein is the AC-limit of $\varepsilon \to 0$ [30, 31].

This system can also be derived from the following Lagrangian

$$L = \sum_n \Big\{ \frac{i}{2}[A_n^*A_n' - A_n(A_n^*)'] + \frac{\Delta\beta}{2}|A_n|^2 + \frac{\gamma_a}{2}|A_n|^4 + \frac{i}{2}[B_n^*B_n' - B_n(B_n^*)'] - \frac{\Delta\beta}{2}|B_n|^2 + \frac{\gamma_b}{2}|B_n|^4 + \varepsilon \mathrm{Re}[2A_nB_{n+1}^* + 2C_1A_nB_n^*] \Big\} \tag{2}$$

and conserves the Hamiltonian

$$H = -\sum_n \Big\{ \frac{\Delta\beta}{2}|A_n|^2 + \frac{\gamma_a}{2}|A_n|^4 - \frac{\Delta\beta}{2}|B_n|^2 + \frac{\gamma_b}{2}|B_n|^4 + \varepsilon \mathrm{Re}[2A_nB_{n+1}^* + 2C_1A_nB_n^*] \Big\} \tag{3}$$

and the total power

$$P = \sum_n (|A_n|^2 + |B_n|^2). \tag{4}$$

With $(A_n, B_n) \propto \exp\{i(nk_x + k_z z)\}$, we obtain the linear dispersion relation $k_z^2 = (\frac{\Delta\beta}{2})^2 + \varepsilon^2(C_1^2 + 1 + 2C_1\cos k_x)$. In the continuum limit, i.e., for $k_x \to 0$, we have $k_z^2 = (\frac{\Delta\beta}{2})^2 + \varepsilon^2(C_1+1)^2$. Instead extending work on the continuum limit beyond [26, 28], this paper focuses on the formation of discrete solitons bifurcating from the uncoupled limit of the system, i.e., from the limit of $\varepsilon \to 0$.

III. EXISTENCE OF DISCRETE SOLITONS

Starting from Eqn. (1) without coupling, i.e. $\varepsilon = 0$

$$\begin{array}{l} iA_n{}' + \frac{\Delta\beta}{2}A_n + \gamma_a|A_n|^2A_n = 0 \\ iB_n{}' - \frac{\Delta\beta}{2}B_n + \gamma_b|B_n|^2B_n = 0 \end{array} \tag{5}$$

for which, in addition to the trivial solutions, we identify nontrivial ones of the form:

$$\begin{array}{l} A_n(z) = a_n e^{ic_n} e^{i[(\frac{\Delta\beta}{2} + \gamma_a a_n^2)z]} \\ B_n(z) = b_n e^{id_n} e^{i[(-\frac{\Delta\beta}{2} + \gamma_b b_n^2)z]} \end{array} \tag{6}$$

where a_n, b_n, (c_n, d_n) are, without loss of generality [30] the real amplitudes (phases).

As we turn on ε, we consider the solution of Eqn. (1) in the form of standing waves as $(A_n, B_n) = (\mathbf{a}_n(z)e^{i\alpha z}, \mathbf{b}_n(z)e^{i\beta z})$, with $\alpha = \frac{\Delta\beta}{2} + a^2\gamma_a$ and $\beta = -\frac{\Delta\beta}{2} + b^2\gamma_b$. Here a, b are amplitudes of $a_n(z)$, $b_n(z)$ respectively corresponding to the $\epsilon = 0$ system. Here instead, $\mathbf{a}_n(z), \mathbf{b}_n(z)$ satisfy

$$\begin{array}{c} i\mathbf{a}_n' = \gamma_a\mathbf{a}_n(a^2 - |\mathbf{a}_n|^2) - \varepsilon(C_1\mathbf{b}_n + \mathbf{b}_{n+1})e^{-i\rho z}, \\ i\mathbf{b}_n' = \gamma_b\mathbf{b}_n(b^2 - |\mathbf{b}_n|^2) - \varepsilon(\mathbf{a}_{n-1} + C_1\mathbf{a}_n)e^{i\rho z}, \end{array} \tag{7}$$

where $\rho = \alpha - \beta = \Delta\beta + a^2\gamma_a - b^2\gamma_b$. For a stationary solution to exist, we must assume that $\rho = 0$, i.e., that the linear detuning in the propagation constant balances the corresponding nonlinear one. The stationary solutions for Eqn. (7) with $(\mathbf{a}_n(z), \mathbf{b}_n(z)) = (a_n, b_n)$, then satisfy

$$\begin{array}{c} \gamma_a a_n(a^2 - |a_n|^2) = \varepsilon(C_1 b_n + b_{n+1}), \\ \gamma_b b_n(b^2 - |b_n|^2) = \varepsilon(a_{n-1} + C_1 a_n). \end{array} \tag{8}$$

When $\varepsilon = 0$, as stated before the solutions of Eqn. (8) are in the form:

$$a_n = a_n^{(0)} = \begin{cases} ae^{ic_n}, & n \in S_1, \\ 0, & n \in \mathbb{Z}/S_1, \end{cases} \qquad b_n = b_n^{(0)} = \begin{cases} be^{id_n}, & n \in S_2, \\ 0, & n \in \mathbb{Z}/S_2, \end{cases} \tag{9}$$

where S_i denote finite sets of nodes of the lattice and $c_n, d_n \in \{0, \pi\}$. Only those waveguides that belong to S_i have a non-zero excitation. For small $\varepsilon \neq 0$, the Jacobian matrix of Eqn. (8) remains invertible, and the solutions of Eqn. (8) are analytic functions of ε around $\varepsilon = 0$ [30, 31]. We can then expand (a_n, b_n) as

$$a_n = a_n^{(0)} + \textstyle\sum_{k=1}^{k=\infty} \varepsilon^k a_n^{(k)}, \qquad b_n = b_n^{(0)} + \textstyle\sum_{k=1}^{k=\infty} \varepsilon^k b_n^{(k)}, \tag{10}$$

In particular, we can solve Eqn. (8) at $\mathrm{O}(\varepsilon)$ to get

$$a_n^{(1)} = \frac{C_1 b_n^{(0)} + b_{n+1}^{(0)}}{\gamma_a(a^2 - 3(a_n^{(0)})^2)}, \qquad b_n^{(1)} = \frac{a_{n-1}^{(0)} + C_1 a_n^{(0)}}{\gamma_b(b^2 - 3(b_n^{(0)})^2)}. \tag{11}$$

While keeping the discussion general, we note here by equating the $O(1)$ terms, that $(a_n^{(0)})^2 = a^2$ and $(b_n^{(0)})^2 = b^2$ for excited nodes. Following the same vein, we can extract the solutions order by order in ε. We now explore the stability of these solutions, by analyzing their linearized eigenvalues.

IV. STABILITY OF DISCRETE SOLITONS

To examine the linear stability of the stationary solutions, we assume small perturbations of the form:

$$\begin{array}{c} A_n(z) = e^{i\alpha z}\{a_n + \delta p_n\} \\ B_n(z) = e^{i\beta z}\{b_n + \delta q_n\} \end{array} \tag{12}$$

where a_n and b_n are stationary solutions that satisfy Eqn. (8), and the term proportional to δ is a small perturbation of order δ. At order $O(\delta)$; δ is a formal parameter, denoting the smallness of the perturbation. We decompose the perturbations, which are complex in nature as $p_n = (r_n + s_n i)e^{\lambda z}$, $q_n = (f_n + h_n i)e^{\lambda z}$, to obtain the linearization equations at $\mathrm{O}(\delta)$:

$$\begin{array}{c} \lambda r_n = \gamma_a(a^2 - a_n^2)s_n - \varepsilon(C_1 h_n + h_{n+1}), \\ -\lambda s_n = \gamma_a(a^2 - 3a_n^2)r_n + \varepsilon(C_1 f_n + f_{n+1}), \\ \lambda f_n = \gamma_b(b^2 - b_n^2)h_n - \varepsilon(s_{n-1} + C_1 s_n), \\ -\lambda h_n = \gamma_b(b^2 - 3b_n^2)f_n + \varepsilon(r_{n-1} + C_1 r_n). \end{array} \tag{13}$$

We rewrite this as

$$\begin{array}{c} \lambda\mathbf{R} = \mathcal{L}_-\mathbf{S} \\ -\lambda\mathbf{S} = \mathcal{L}_+\mathbf{R} \end{array} \tag{14}$$

where $\mathbf{R} = (\cdots, r_{n-1}, f_{n-1}, r_n, f_n, \cdots)^T$, $\mathbf{S} = (\cdots, s_{n-1}, h_{n-1}, s_n, h_n, \cdots)^T$ and $\mathcal{L}_\pm$ are infinite-dimensional symmetric tri-diagonal matrices, which consist of elements

$$\begin{array}{c} (\mathcal{L}_-)_{n,n} = \begin{pmatrix} \gamma_a(a^2 - a_n^2) & -\varepsilon C_1 \\ -\varepsilon C_1 & \gamma_b(b^2 - b_n^2) \end{pmatrix} \\ (\mathcal{L}_+)_{n,n} = \begin{pmatrix} \gamma_a(a^2 - 3a_n^2) & \varepsilon C_1 \\ \varepsilon C_1 & \gamma_b(b^2 - 3b_n^2) \end{pmatrix} \\ (\mathcal{L}_\pm)_{n,n+1} = \begin{pmatrix} 0 & \pm\varepsilon \\ 0 & 0 \end{pmatrix} = (\mathcal{L}_\pm)_{n,n-1}^T. \end{array} \tag{15}$$

We can further write Eqns. (14) in the form:

$$\lambda \mathbf{\Psi} = \mathcal{J}\mathcal{H}\mathbf{\Psi}, \tag{16}$$

where $\mathbf{\Psi} = (\cdots, r_n, f_n, s_n, h_n, \cdots)^T$ is the eigenvector, $\mathcal{H}$ is defined as

$$\mathcal{H}_{n,m} = \begin{pmatrix} (\mathcal{L}_+)_{n,m} & \mathbf{0} \\ \mathbf{0} & (\mathcal{L}_-)_{n,m} \end{pmatrix} \tag{17}$$

and the skew-symmetric matrix $\mathcal{J}$ consists of 4×4 blocks of the form:

$$\begin{pmatrix} 0 & 0 & 1 & 0 \\ 0 & 0 & 0 & 1 \\ -1 & 0 & 0 & 0 \\ 0 & -1 & 0 & 0 \end{pmatrix} \tag{18}$$

Let's first consider the uncoupled case when $\varepsilon = 0$. Since the coupling term is zero, the analysis is independent of which population of the waveguides is excited. For a total of K excited waveguides A_n (B_n), the eigenvalues μ of $\mathcal{H}\mathbf{\Phi} = \mu\mathbf{\Phi}$ consist of exactly K eigenvalues $\mu = -2\gamma_a a^2$ ($\mu = -2\gamma_b b^2$) from $\mathcal{L}_+$ and K eigenvalues of $\mu = 0$ from $\mathcal{L}_-$. Eventually these will map to K double zeros of λ. For the remaining infinite unexcited (i.e., vanishing) A_ns (B_ns), we will get an infinite number of $\mu = \gamma_a a^2$ ($\mu = \gamma_b b^2$) from both $\mathcal{L}_\pm$, which will eventually map to infinite pairs of $\lambda = \pm i\gamma_a a^2$ ($\lambda = \pm i\gamma_b b^2$).

As we turn on ε, the infinite number of $\lambda = \pm i\gamma_a a^2$ ($\lambda = \pm i\gamma_b b^2$), will form the branches of the continuous spectrum, actually with plane wave eigenfunctions $p_n, q_n \propto e^{\pm i(kn - \omega z)}$. The corresponding eigenvalues $\lambda = i\omega$ satisfy

$$(\pm\omega - \gamma_a a^2)(\pm\omega - \gamma_b b^2) = \varepsilon^2(C_1^2 + 1 + 2C_1\cos(k)). \tag{19}$$

Now let us focus on how the finite number of zero eigenvalues move (possibly) away from $\lambda = 0$, as we turn on ε. We write Eqn. (14) as,

$$\lambda^2 \mathbf{S} = -\mathcal{L}_+\mathcal{L}_-\mathbf{S} \tag{20}$$

and notice that $\mathcal{L}_+$ is invertible when $\varepsilon = 0$, so there exists ε_0, such that when $0 \le \varepsilon < \varepsilon_0$, $\mathcal{L}_+$ is still invertible. Then, we have

$$\lambda^2 \mathcal{L}_+^{-1}\mathbf{S} = -\mathcal{L}_-\mathbf{S}. \tag{21}$$

Forming the inner product of both sides of Eqn. (21) with $\mathbf{S}$, we get

$$\lambda^2 = -\frac{< \mathbf{S}, \mathcal{L}_-\mathbf{S} >}{< \mathbf{S}, \mathcal{L}_+^{-1}\mathbf{S} >}, \tag{22}$$

where the inner product is defined as $< \mathbf{u}, \mathbf{v} >= \sum_n \bar{u}_n v_n$.

As mentioned before we can expand (a_n, b_n) in powers of ε, and similarly we can also expand $\mathcal{L}_\pm$, $\mathbf{S}$, etc. In particular, if $\mathbf{S_a}$ is the eigenvector of $\mathcal{L}_-$ corresponding to μ_a, such that $\lim_{\varepsilon\to 0}\mu_a = 0$, then

$$\lim_{\varepsilon\to 0} < \mathbf{S_a}, \mathcal{L}_+^{-1}\mathbf{S_a} >=< \mathbf{S_a^{(0)}}, (\mathcal{L}_+^{-1})^{(0)}\mathbf{S_a^{(0)}} >\neq 0. \tag{23}$$

where $(\mathcal{L}_+^{-1})^{(0)}$ will be a diagonal matrix with

$$(\mathcal{L}_+^{-1})^{(0)}_{n,n} = \begin{pmatrix} \frac{1}{\gamma_a(a^2 - 3(a_n^{(0)})^2)} & 0 \\ 0 & \frac{1}{\gamma_b(b^2 - 3(b_n^{(0)})^2)} \end{pmatrix}. \tag{24}$$

Then the leading order in ϵ of λ^2 will be

$$\lambda^2 = -\frac{\mu_a < \mathbf{S_a^{(0)}}, \mathbf{S_a^{(0)}} >}{< \mathbf{S_a^{(0)}}, (\mathcal{L}_+^{-1})^{(0)}\mathbf{S_a^{(0)}} >} + O(\varepsilon^2). \tag{25}$$

The problem which remains is to find the leading order eigenvalues and eigenvectors of $\mathcal{L}_-$. To compute this, we expand $\mathcal{L}_-$ as

$$(\mathcal{L}_-)_{n,n} = \begin{pmatrix} \gamma_a(a^2-a_n^2) & -\varepsilon C_1 \\ -\varepsilon C_1 & \gamma_b(b^2-b_n^2) \end{pmatrix} = (\mathcal{L}_-^{(0)})_{n,n} + \varepsilon(\mathcal{L}_-^{(1)})_{n,n} + O(\varepsilon^2) \tag{26}$$

$$= \begin{pmatrix} \gamma_a(a^2-(a_n^{(0)})^2) & 0 \\ 0 & \gamma_b(b^2-(b_n^{(0)})^2) \end{pmatrix} + \varepsilon \begin{pmatrix} -2\gamma_a a_n^{(0)} a_n^{(1)} & -C_1 \\ -C_1 & -2\gamma_b b_n^{(0)} b_n^{(1)} \end{pmatrix} + O(\varepsilon^2)$$

$$(\mathcal{L}_-)_{n,n+1} = \mathbf{0} + \varepsilon \begin{pmatrix} 0 & -1 \\ 0 & 0 \end{pmatrix} = (\mathcal{L}_-)_{n,n-1}^T. \tag{27}$$

and project $\mathcal{L}_-\mathbf{S_a} = \mu_a \mathbf{S_a}$ on to the kernel of $\mathcal{L}_-^{(0)}$, we have

$$\mathcal{L}_-^{(0)}\mathbf{S_a^{(0)}} = \mu_a^{(0)}\mathbf{S_a^{(0)}} = 0, \tag{28}$$

$$\mathcal{L}_-^{(0)}\mathbf{S_a^{(1)}} + \mathcal{L}_-^{(1)}\mathbf{S_a^{(0)}} = \mu_a^{(1)}\mathbf{S_a^{(0)}}. \tag{29}$$

Here $\mathbf{S_a^{(0)}}$ can be written as combinations of basis elements in the kernel of $\mathcal{L}_-^{(0)}$, i.e. $\mathbf{S_a^{(0)}} = \sum_{k=1}^{K} c_k e_k$, where the basis elements e_k can be chosen as $e_k = (\cdots, 0, \pm 1, 0, \cdots)^T$, where the "$\pm 1$" is located at the kth excited site and the sign is chosen to be the same as the anti-continuum limit. Then, we obtain

$$\mathbf{M}c = \mu^{(1)}c \tag{30}$$

where the $K \times K$ matrix $\mathbf{M}$ with elements

$$\mathbf{M}_{m,n} = < e_m, \mathcal{L}_-^{(1)} e_n > . \tag{31}$$

Once we have the eigenvalue and eigenvector of $\mathbf{M}$, then by Eqn. (25) we get

$$\lambda^2 = -\frac{\mu_a^{(1)} < \mathbf{S_a^{(0)}}, \mathbf{S_a^{(0)}} >}{< \mathbf{S_a^{(0)}}, (\mathcal{L}_+^{-1})^{(0)} \mathbf{S_a^{(0)}} >} \varepsilon + O(\varepsilon^2). \tag{32}$$

We will provide a series of concrete examples of this calculation for configurations with 2-4 sites, in the section below titled Computations.

V. COMPUTATIONS

In the next three subsections we will discuss setups with two, three and four excited sites, respectively. We denote excited nodes of $a_n^{(0)}$ and $b_n^{(0)}$ as "+" if they are positive, "−" if they are negative, and use parameters $C_1 = 2,\ a = 1,\ b = 1, \Delta\beta = 1,\ \gamma_a = 1,\ \gamma_b = 2$ unless stated otherwise. We will first identify the stationary solutions using Eqn. (8) by means of fixed-point Newton iterations and parameter continuation on ε starting from $\varepsilon = 0$. Then, we will identify the spectrum of the linear stability analysis for these stationary solutions numerically, by solving the full matrix eigenvalue problem of Eqn. (16). Lastly, we will compare the eigenvalues that bifurcate from zero –these are the ones that are potentially responsible for emerging instabilities– with their leading order theoretical approximations provided by Eqn. (32). Finally, when the solutions are identified to be spectrally unstable, we will also study their evolutionary dynamics, to explore the outcome of this instability upon propagation in z.

A. Two excited sites

Let us first consider the case where the only nonzero entries of $(a_n^{(0)}, b_n^{(0)})$ are

$$(a_0^{(0)}, b_0^{(0)}) = (ae^{ic_0}, be^{id_0}), \tag{33}$$

with $c_0, d_0 \in \{0, \pi\}$. From Eqn. (11), we get the nonzero entries for $(a_n^{(1)}, b_n^{(1)})$ are

$$(a_n^{(1)}, b_n^{(1)}) = \begin{cases} (\frac{be^{id_0}}{\gamma_a a^2}, 0), & n = -1 \\ (\frac{C_1 be^{id_0}}{-2\gamma_a a^2}, \frac{C_1 ae^{ic_0}}{-2\gamma_b b^2}), & n = 0 \\ (0, \frac{ae^{ic_0}}{\gamma_b b^2}), & n = 1. \end{cases} \tag{34}$$

From Eqn. (31), we obtain

$$\mathbf{M} = C_1 e^{i(d_0-c_0)} \begin{pmatrix} \frac{b}{a} & -1 \\ -1 & \frac{a}{b} \end{pmatrix}. \tag{35}$$

$\mathbf{M}$ has zero eigenvalue with eigenvector $(a,b)^T$, which will map to a double zero of λ. This corresponds to the phase (or gauge) invariance of the model, associated with the U(1) symmetry. The nonzero eigenvalue $C_1\cos(d_0-c_0)(\frac{a}{b}+\frac{b}{a})$ has eigenvector $(b,-a)^T$, so the leading order of λ^2 is

$$\lambda^2 \approx \frac{C_1(\frac{b}{a}+\frac{a}{b})(a^2+b^2)}{\frac{b^2}{2\gamma_a a^2}+\frac{a^2}{2\gamma_b b^2}}\cos(c_0-d_0)\varepsilon \tag{36}$$

That means if $\gamma_a = \gamma_b = \gamma$, $\lambda^2 \approx \varepsilon\cos(c_0-d_0)\gamma C_1 c$, where $c = \frac{2(b/a+a/b)(a^2+b^2)}{b^2/a^2+a^2/b^2}$ is a positive number. So if $\cos(c_0-d_0)\gamma C_1 > 0$ we will have an unstable stationary solution.

As shown in both Fig. 1 and Fig. 2, a pair of eigenvalues will bifurcate from zero as we turn on the coupling ε. In the case in which the two excited sites have the same sign when $\varepsilon = 0$ in Fig. 1, as we increase ε, the pair of eigenvalues move along the real axis as predicted by the leading order and the stationary solution becomes unstable. This is reminiscent of the standard DNLS case of $C_1 = 1$ [30], although we should point out based on the above results that this would change via a change of the sign of C_1. The middle panels of Fig. 1 from left to right show, for $\varepsilon = 0.2$, the stationary solution, its corresponding linearization spectrum and the unstable eigenvector respectively. Here, it is evident that in addition to the zero eigenvalue-pair (due to the phase invariance) and the real pair (the instability discussed above), two bands of continuous spectrum are forming, per the dispersion relation discussed in Eqn. (19).

If we now perturb the stationary solution along the unstable eigendirection by initially adding to it a small (amplitude of 0.1%) contribution of the unstable eigenvector, we obtain the dynamical evolution shown in the bottom panels of Fig. 1. The contour plots in the spatial (n) and the propagation variable (z), clearly shows that the instability evolves into a robust periodic orbit. Since we are only showing the modulus of the waveform here (absorbing an additional $e^{-i\beta z}$ factor), this suggests that the nature of the solution is quasi-periodic.

On the other hand, in Fig. 2 the two components are out of phase when uncoupled. As we increase ε, a pair of eigenvalues bifurcates from zero and moves along the imaginary axis, so the stationary solution is stable; again this is in line with the DNLS result of [30] which is hereby generalized for $C_1 \neq 1$. At $\varepsilon \approx 0.058$ the purely imaginary discrete pair of eigenvalues collides with the first band edge of the continuous spectrum and becomes a complex quartet, while the stationary solution becomes unstable, via the resulting oscillatory instability. As the eigenvalue pairs return to the imaginary axis for $\varepsilon \approx 0.079$, the solution becomes stable again until it reaches the second band edge of the continuum spectrum. So instead of being purely imaginary for all ε, here we see that the discrete eigenvalues become resonant with the continuous spectrum and yield intervals of oscillatory instability, associated with complex eigenvalue quartets, such as the one for $0.058 < \varepsilon < 0.079$. Perturbing the stationary solution with 10% of its amplitude in the unstable direction results in the dynamics shown in the bottom panels of Fig. 2. Importantly, the instability dynamics still results in a robust quasi-periodic breather type of waveform eventhough the behavior of the eigenvalues manifests. in a different manner.

B. Three excited sites

We now explore the case with three excited sites, i.e., at the AC limit (a_n, b_n) of the form:

$$(a_n^{(0)}, b_n^{(0)}) = \begin{cases} (ae^{ic_{-1}},\ 0), & n=-1, \\ (ae^{ic_0},\ be^{id_0}), & n=0, \end{cases} \tag{37}$$

From Eqn. (11), the nonzero entries for the first order expansion of (a_n, b_n) will be

$$(a_n^{(1)}, b_n^{(1)}) = \begin{cases} (\frac{be^{id_0}}{-2\gamma_a a^2},\ \frac{C_1 ae^{ic_{-1}}}{\gamma_b b^2}), & n=-1, \\ (\frac{C_1 be^{id_0}}{-2\gamma_a a^2},\ \frac{ae^{ic_{-1}}+C_1 ae^{ic_0}}{-2\gamma_b b^2}), & n=0, \\ (0,\ \frac{ae^{ic_0}}{\gamma_b b^2}), & n=1. \end{cases} \tag{38}$$

Using Eqn. (31), denoting $s_1 = e^{i(d_0-c_0)}$, $s_2 = e^{i(c_0-c_{-1})}$, we find

$$\mathbf{M} = s_1 \begin{pmatrix} \frac{b}{a}s_2 & 0 & -s_2 \\ 0 & \frac{C_1 b}{a} & -C_1 \\ -s_2 & -C_1 & \frac{a}{b}(C_1+s_2) \end{pmatrix}. \tag{39}$$

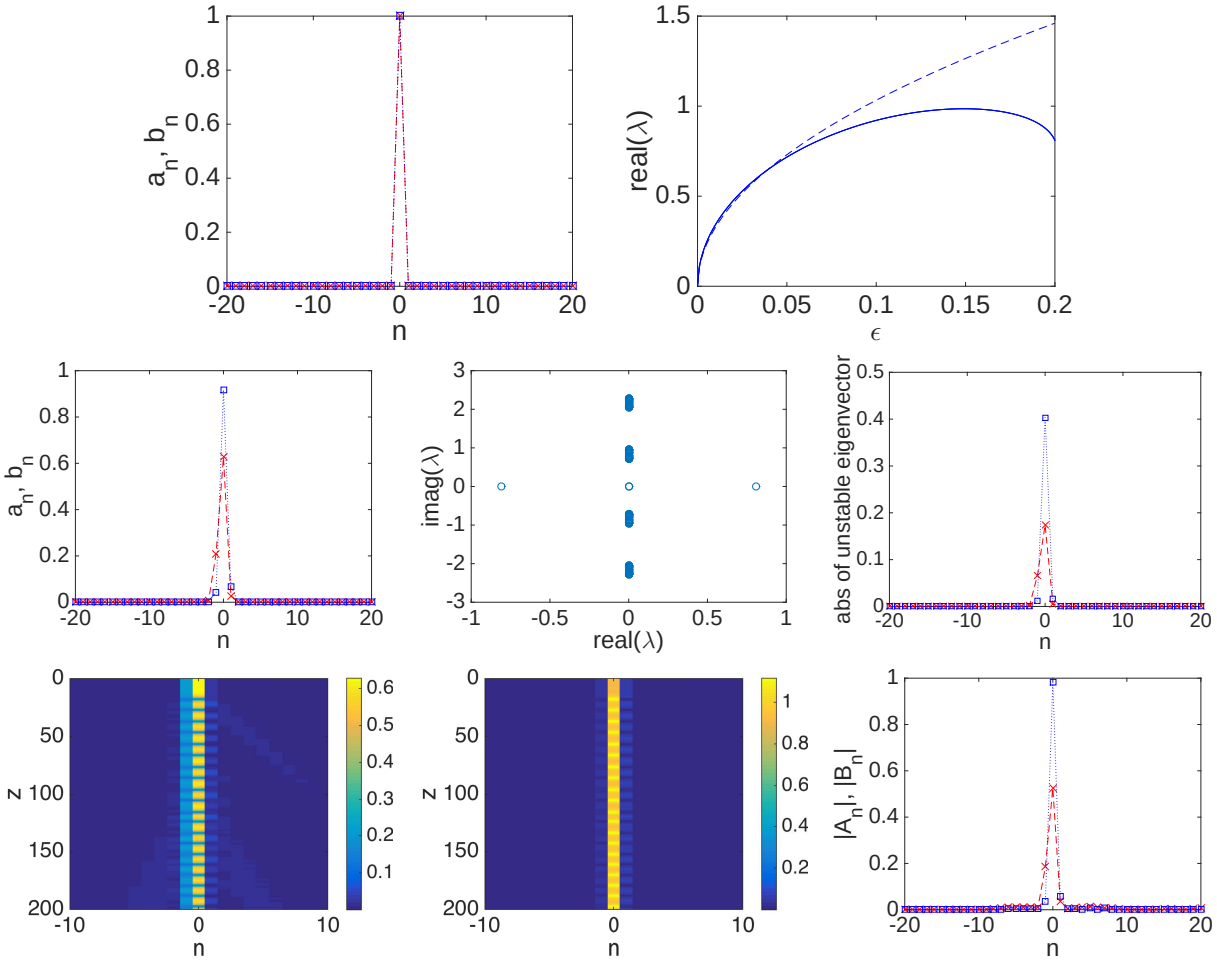

FIG. 1: The stationary solution profiles of a_n in red crosses and b_n in blue squares is shown. Starting from $\varepsilon = 0$ on the top left panel, continuously increasing up to $\varepsilon = 0.2$, we find the stationary solution in the middle left panel and its linear stability on the central middle row panel. In top right panel, the real part of the relevant unstable eigenvalue is shown as a function of ε by the solid line, and the dashed line indicates its leading order theoretical approximation from the analysis of section IV. At $\varepsilon = 0.2$, if we perturb the stationary solution with the unstable eigenvector (in middle right panel) with an amplitude of 0.1% of the stationary solution, we find the evolution of $|A_n|$ and $|B_n|$ shown as a contour plot in the spatial (n) and evolution (z) variables in the bottom left and bottom middle panels. The profiles at $z = 200$ are shown in the bottom right panel.

Again, as in the case of two excited cases, $\mathbf{M}$ has a 0 eigenvalue with eigenvector $(a, a, b)^T$ that corresponds to the phase invariance of the underlying binary waveguide model. The other two eigenvalues are

$$\mu_\pm = s_1 \frac{1}{2}\Big[(a/b + b/a)(C_1 + s_2) \pm \sqrt{(a/b + b/a)^2(C_1 + s_2)^2 - 4s_2C_1(b^2/a^2 + 2)}\Big] \tag{40}$$

with corresponding eigenvectors $(\frac{1}{b/a - s_2\mu_\pm}, \frac{C_1}{C_1 b/a - \mu_\pm}, 1)$. So according to Eqn. (32), the leading order of λ^2 will be

$$\lambda^2 \approx \varepsilon \frac{\mu_\pm(\frac{1}{(b/a - s_2\mu_\pm)^2} + \frac{C_1^2}{(C_1 b/a - \mu_\pm)^2} + 1)}{\frac{1}{(b/a - s_2\mu_\pm)^2(2\gamma_a a^2)} + \frac{C_1^2}{(C_1 b/a - \mu_\pm)^2(2\gamma_a a^2)} + \frac{1}{2\gamma_b b^2}}. \tag{41}$$

In the simpler case of $\gamma_a = \gamma_b = \gamma$, and $a = b$,

$$\lambda^2 \approx \varepsilon 2a^2\gamma s_1[(C_1 + s_2) \pm \sqrt{(C_1 + s_2)^2 - 3s_2C_1}] =: \varepsilon 2a^2\gamma s_1 c_\pm, \tag{42}$$

where λ^2 depends on $c_\pm$, in addition to the product $\varepsilon 2a^2\gamma s_1$. In order to gauge the role of C_1 in modifying the relevant eigenvalues from the DNLS limit of $C_1 = 1$, Fig. 3 shows $c_\pm$ as increasing functions of C_1. The graphs have

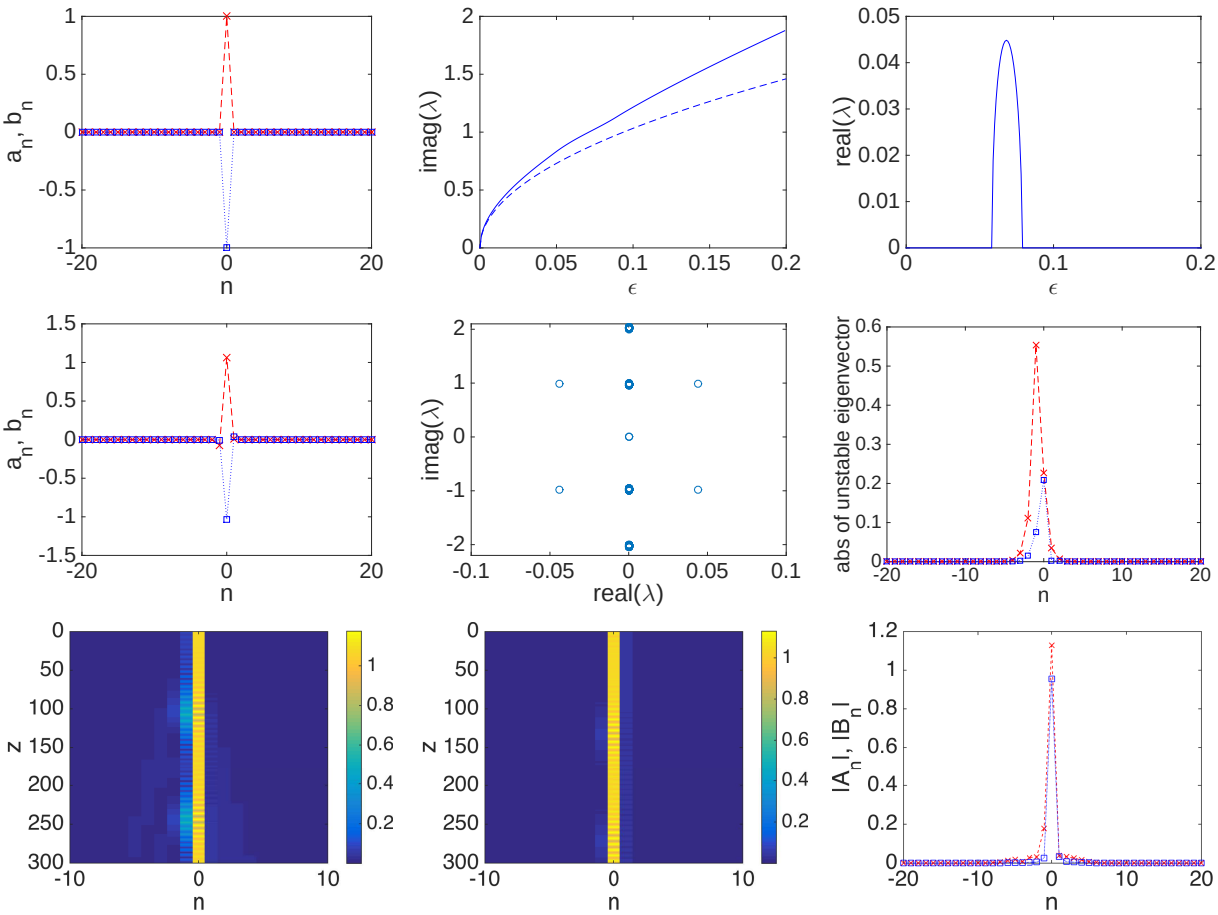

FIG. 2: Similar to Fig. 1, but now for the case where the two excited sites for a_n and b_n are out of phase. Starting from $\varepsilon = 0$ on the top left panel, we continuously increase ε up to $\varepsilon = 0.2$. The real and imaginary part of the relevant eigenvalue that bifurcates from zero are shown in top middle and top right panels respectively, where the dash line is the leading order theoretical approximation of Section IV. As ε increases, a pair of eigenvalues bifurcates from zero and moves along the imaginary axis. For $0.058 < \varepsilon < 0.079$, the imaginary eigenvalues collide with the continuous spectrum and yield a complex quartet (associated with an oscillatory instability –hence the existence of a nonzero real part in the top right panel within this interval–). The stationary solution at $\varepsilon = 0.07$ is shown in middle left panel. The spectrum of linear stability and the most unstable eigenmode are observed in the central and the right panel of the middle row. Finally, with perturbation amplitude 10% of the stationary state, the unstable dynamics of the state is shown in the bottom panels via contour plots (as in Fig. 1), and the modulus profile at the final propagation distance of $z = 300$.

an asymptotic behavior described by the straight lines $y = s_2$ and $y = 2x + s_2$. It can again be seen that C_1 plays a critical role in the stability properties, with its sign variation inducing a change from real to imaginary of one of the relevant eigenvalue pairs. It is interesting to point out that generally, increasing the magnitude of the parameter C_1 leads to an increase of $c_\pm$ rendering the configuration more prone to potential instabilities.

We now discuss the four different potential combinations of signs of s_1, s_2. We will denote $(a_{-1}^{(0)} a_0^{(0)}, b_{-1}^{(0)} b_0^{(0)})$ only by the sign of each of the elements.

- $(++, 0+)$:

  The stationary solution for $\varepsilon = 0$ is shown in top left panel of Fig. 4. In this case $s_1 = s_2 = +1$. This in phase configuration results into two pairs of real eigenvalues. This can be confirmed by the top right panel of Fig. (4), where we get two unstable eigenvalue pairs as functions of ε that are well predicted by their leading order approximations in dashed line, at least for small values of ε. When ε gets to be large, then the eigenvalues show a decreasing tendency in their variation over ε suggesting that higher order terms become significant. At $\varepsilon = 0.2$, we find the stationary solution and its linear stability spectrum in the middle left and center panels respectively. If we perturb this stationary solution with the most unstable eigenvector in middle right panel, of amplitude 1% of the stationary state, we get the evolution of $|A_n|$, $|B_n|$ shown in the bottom left and middle

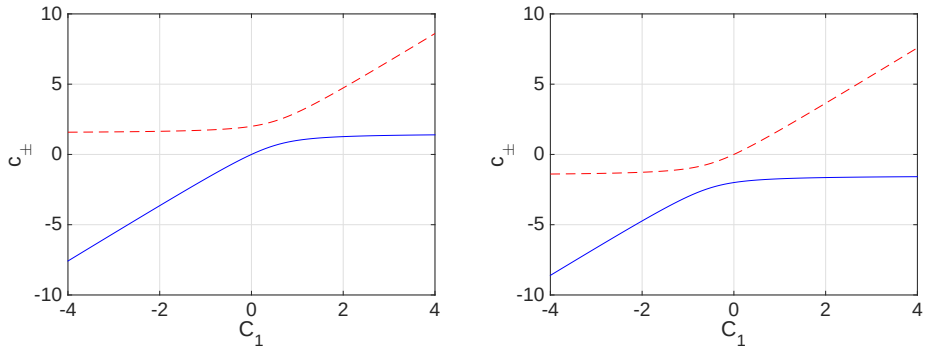

FIG. 3: $c_\pm$ entering the expression of Eq. (42), is given as a function of C_1. The left panel is for $s_2 = 1$ and the right panel is for $s_2 = -1$. The red dashed line indicates c_+, while the blue solid indicates c_-.

panels respectively. The profile of $|A_n|$, $|B_n|$ at $z = 200$ is shown in bottom right panel. Once again, we can observe the formation of a robust periodic breathing state, in the (modulus) evolution dynamics.

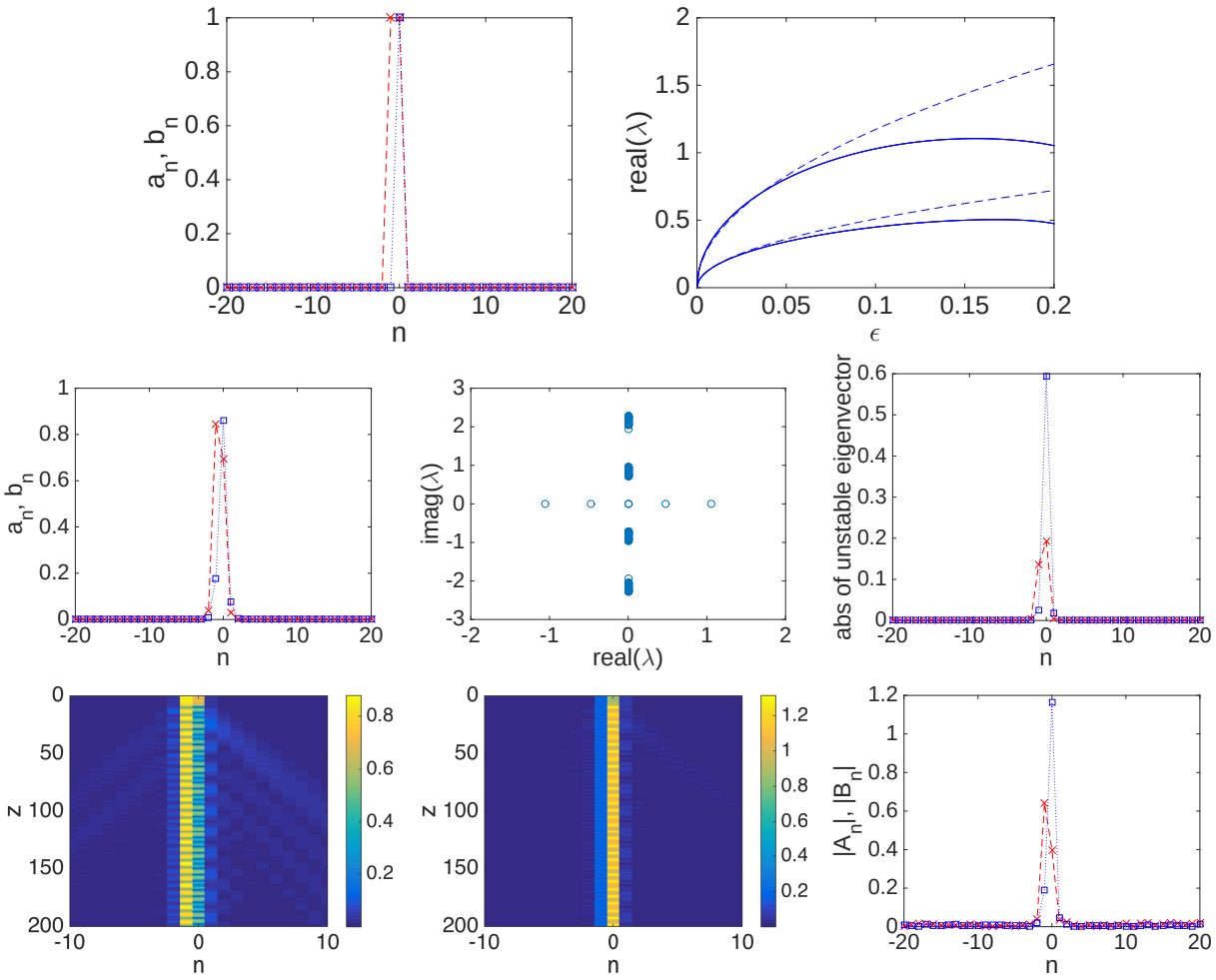

FIG. 4: Similar to Fig. 1 but for the case of the 3-excited sites in the form $(++, 0+)$. Here the main difference is that there are two real eigenvalue pairs (as opposed to in Fig. 1) responsible for the instability.

- $(-+, 0+)$:

  In this case $s_1 = 1$, $s_2 = -1$, the two pairs of eigenvalues that bifurcate from zero will consist of one pair moving

along the real axis and the other pair moving along the imaginary axis. As shown in Fig. 5, both the one moving along real axis in the top middle panel and the one moving along imaginary axis in top right panel are well predicted by their leading order approximations in dashed lines for small values of ε. The stationary solution at $\varepsilon = 0.1$, its spectrum and the unstable eigenvector are shown in the middle panels. For larger values of ε, the pair of eigenvalues that moves along the imaginary axis will collide with the continuous spectrum, yielding additional potential oscillatory instabilities (not considered herein, given the instability of this state immediately off of the AC limit). The dynamics with 1% perturbation in the unstable direction are shown in the bottom panels, where the amplitude of the localized excited cites oscillate but this time in a less regular fashion.

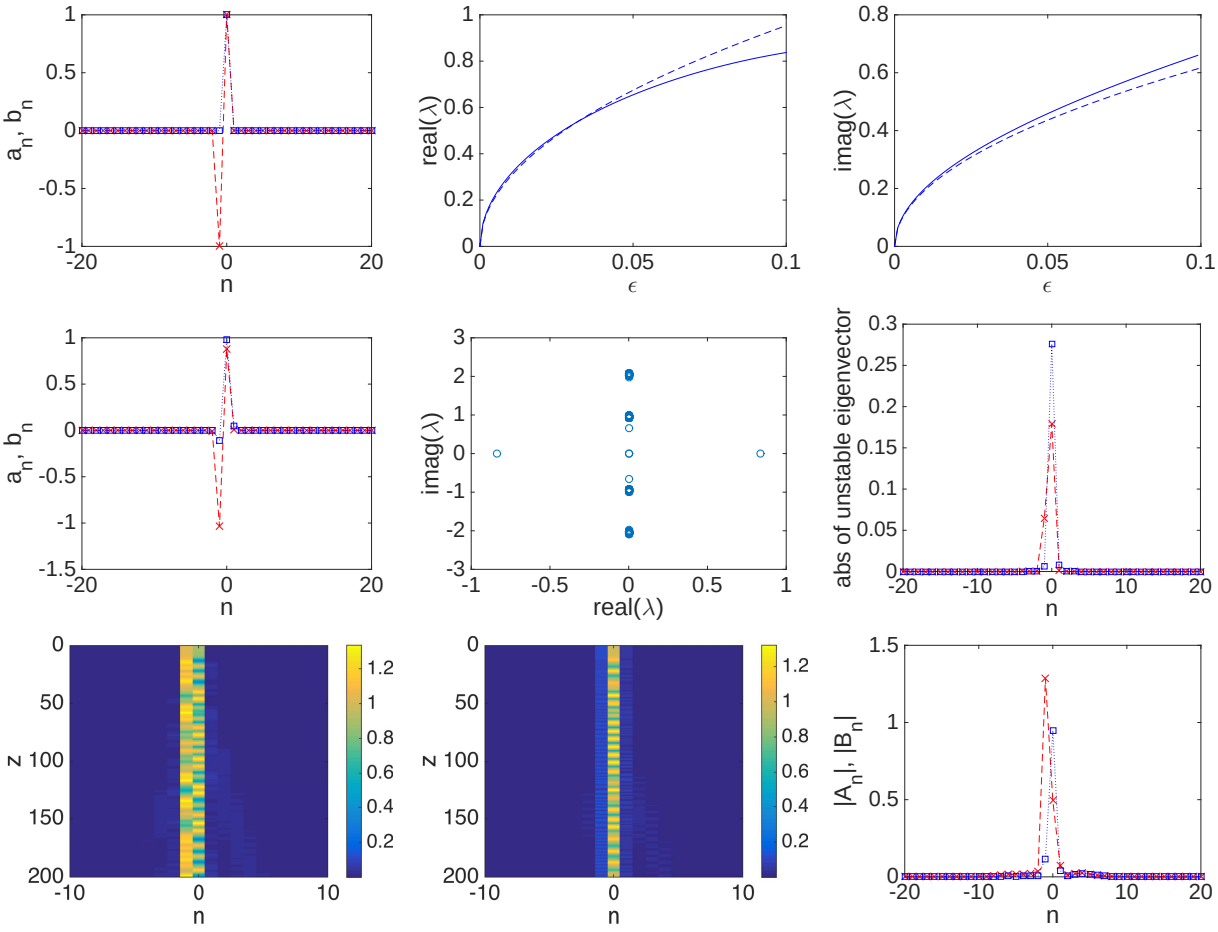

FIG. 5: The $(-+,0+)$ solution profile is shown at the AC limit (top left panel) and for $\varepsilon = 0.1$ (middle left panel). The dependence of the one real and one imaginary pair emerging in this case as a function of ε is shown in the top middle and top right panels while the full spectral plane for $\varepsilon = 0.1$ is shown in the middle panel of the second row. The bottom panels show the unstable dynamics and the final propagation distance of $z = 200$.

- $(+-,0+)$:

  In this case $s_1 = -1$, $s_2 = -1$. This is a scenario quite similar to the previous one, leading to a real and an imaginary eigenvalue pair and a configuration immediately unstable off of the AC limit. For this reason, we do not focus on it further here.

- $(++,0-)$:

  In this case $s_1 = -1$, $s_2 = 1$. The two pairs of eigenvalues are both moving along the imaginary axis, as shown in Fig. 6. Again this is well captured by the leading order approximations, for small values of ε. This effective "out of phase" configuration (i.e., with adjacent waveguides bearing alternating 0 and π phases) is spectrally stable for small values of ε, similarly to its corresponding DNLS cousin [30]. Yet, it is subject to up to 2 quartets of oscillatory instabilities, as ε is increased due to collisions of the relevant pairs of imaginary eigenvalues growing from 0 with the continuous spetrum.

It is relevant to note that we have confirmed the results of Fig. 3 for the full system. For instance, in the present setting, we also considered the case of $C_1 = -1,\ a = 1,\ b = 1, \Delta\beta = 0,\ \gamma_a = 1,\ \gamma_b = 1$, observing that in line with the results of the latter figure, instead of 2 imaginary eigenvalue pairs, in that case a real and an imaginary pair arise. The predictions of the theory for small values of ε were again found to be in good agreement with the full numerical results.

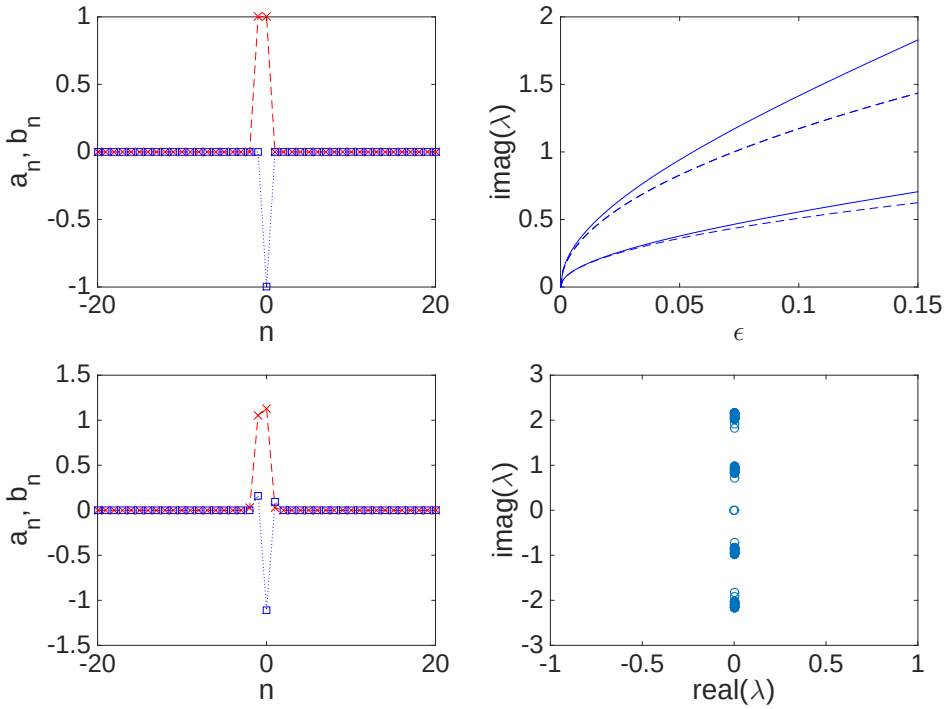

FIG. 6: Profile of the $(++,0-)$ state for $\varepsilon = 0$ (top left) and $\varepsilon = 0.15$ (bottom left). The spectral plane of the latter is shown in the bottom right, while the imaginary eigenvalues (predicted by theory through the dashed lines, and computed numerically in the solid lines) emanating from 0 are shown in the top right.

C. Four excited sites

Finally, we consider some prototypical families of configurations where the nonzero entries span 4 sites. In that case, we have

$$(a_n^{(0)}, b_n^{(0)}) = \begin{cases} (ae^{ic_0},\ be^{id_0}),\ n = 0, \\ (ae^{ic_1},\ be^{id_1}),\ n = 1, \end{cases} \tag{43}$$

then

$$(a_n^{(1)}, b_n^{(1)}) = \begin{cases} (\frac{be^{id_0}}{\gamma_a a^2}, & 0), & n = -1 \\ (\frac{C_1 be^{id_0} + be^{id_1}}{-2\gamma_a a^2}, & \frac{C_1 ae^{ic_0}}{-2\gamma_b b^2}), & n = 0, \\ (\frac{C_1 be^{id_1}}{-2\gamma_a a^2}, & \frac{ae^{ic_0} + C_1 ae^{ic_1}}{-2\gamma_b b^2}), & n = 1, \\ (0, & \frac{ae^{ic_1}}{\gamma_b b^2}) & n = 2. \end{cases} \tag{44}$$

Letting $s_1 = e^{i(c_0 - d_0)}$, $s_2 = e^{i(d_0 - d_1)}$, $s_3 = e^{i(d_1 - c_1)}$, the matrix determining the stability of the configuration now reads:

$$\mathbf{M} = s_1 \begin{pmatrix} (C_1 + s_2)\frac{b}{a} & -C_1 & 0 & -s_2 \\ -C_1 & \frac{C_1 a}{b} & 0 & 0 \\ 0 & 0 & \frac{s_3 C_1 b}{a} & -s_3 C_1 \\ -s_2 & 0 & -s_3 C_1 & (s_3 C_1 + s_2)\frac{a}{b} \end{pmatrix}. \tag{45}$$

We only consider, for illustration purposes, the following two cases

- $(++,++)$:

  As seen in Fig. 7, there will be three unstable pairs of eigenvalues bifurcating from zero, all of which are well predicted by their leading order theoretical approximations in the dashed lines in top right panel. Hence, this configuration is highly unstable, following also the general prediction of the theory of [30] for $C_1 = 1$, suggesting that a configuration with n in-phase excited sites will lead to $n-1$ real eigenvalue pairs.

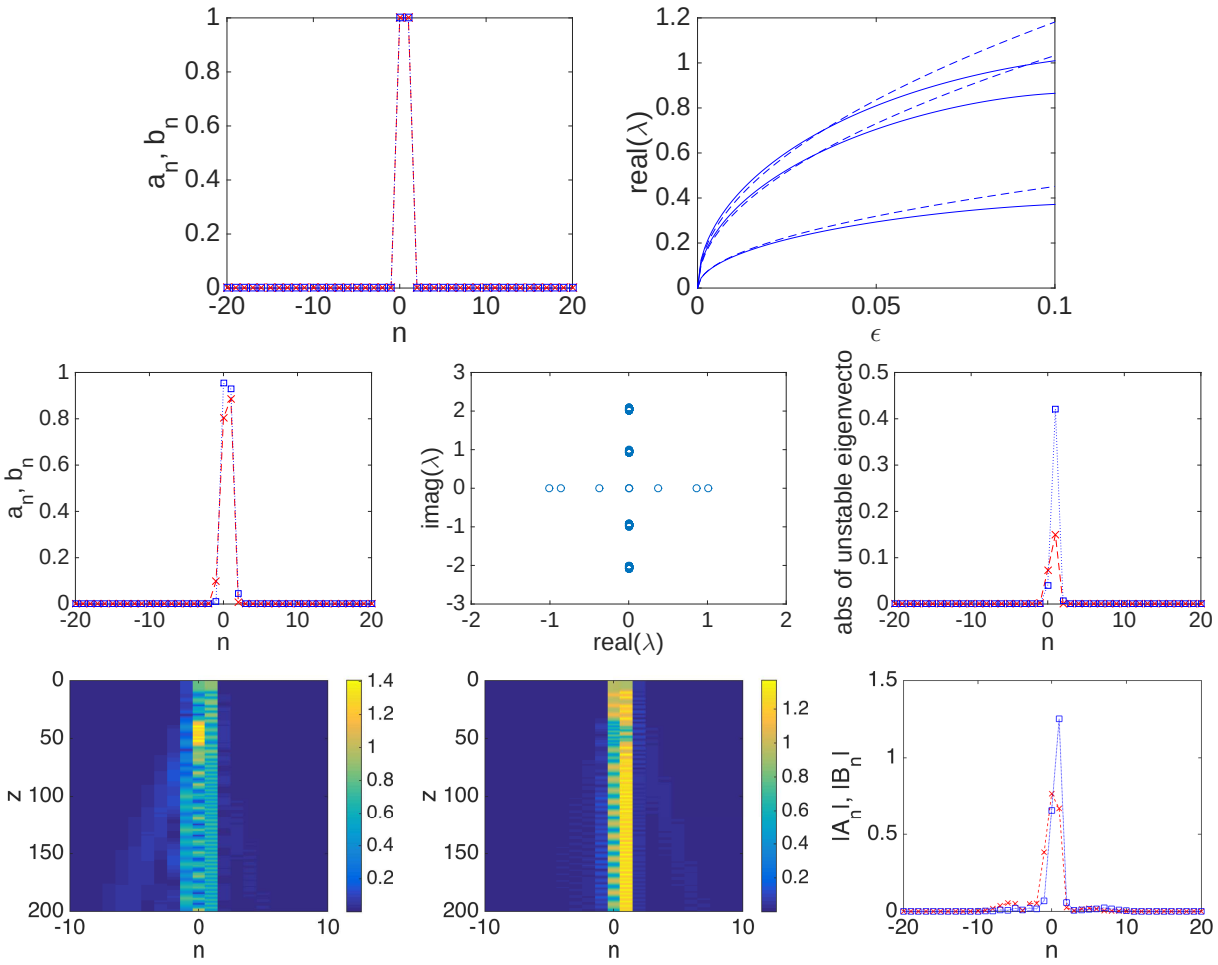

FIG. 7: Similar to Fig. 6, but now for the configuration $(++,++)$ bearing three real eigenvalue pairs (whose real part is shown in the top right). The configuration and the associated spectral plane are shown in the middle panels of the figure for $\varepsilon = 0.1$. The unstable dynamics are in the bottom panels with the modulus profile at $z = 200$ at bottom right. While the dynamics is not genuinely periodic in the modulus, it is fairly proximal to that for sufficiently long times.

- $(++,--)$:

  In this configuration, again bearing alternating phases, we have three imaginary eigenvalue pairs bifurcate from zero, as shown in Fig. 8. As ε increases, the largest one will collide with the edge of the continuous spectrum first and become unstable. As ε increases further, the second one will collide for larger values of ε, hence in the top right panel, there are two humps of the real part of the eigenvalues associated with these two intervals of oscillatory instabilities. The presence of three imaginary eigenvalues in this case can yield up to three distinct sets of oscillatory instabilities and corresponding eigenvalue quartets.

VI. CONCLUSIONS AND FUTURE CHALLENGES

In the present work, we have considered a binary waveguide system in the vicinity of the anti-continuous limit. We have developed our theoretical analysis of the existence and stability of few site configurations in as general a manner as possible. We were able to parametrically characterize the perturbed configurations (at the level of existence) and

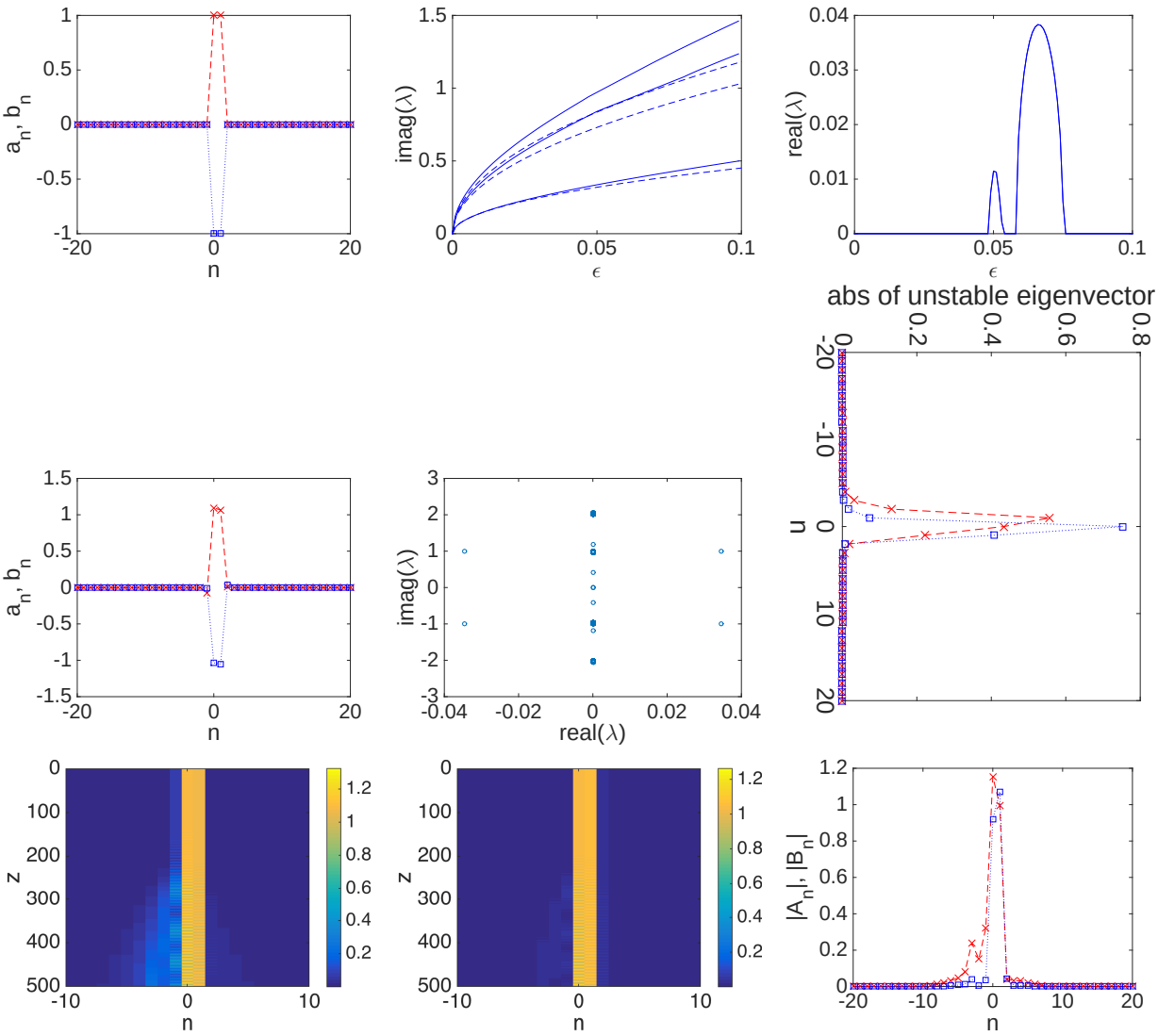

FIG. 8: Similar to the previous figure but now for the configuration of the form $(++,--)$. Here there are three imaginary eigenvalues shown in the top middle, but their collisions with the continuous spectrum give rise to quartets that possess real parts shown in the top right panel. From left to right, the middle row shows the stationary solution profile and spectral plane and the unstable eigenmode for $\varepsilon = 0.07$. The bottom panels are the unstable dynamics and the modulus profile at $z = 500$.

their corresponding linearization eigenvalues (at the level of spectral stability). While the qualitative characteristics of the principal cases we considered were reminiscent of regular waveguide chains, we illustrated that this is strongly dependent (as is even the conclusion of stability/instability itself) on the sign and magnitude of the binary coupling parameter C_1. We illustrated that variations of this parameter can even switch specific configurations from stable to unstable or vice-versa. Whenever our examined configurations were found to be unstable, we also used direct numerical simulation in order to study their dynamical evolution. For instance, for two excited nodes the relevant states result in robust breathing evolution which persists for long propagation intervals. As the number of excited nodes increases, the more complicated interactions of the excited nodes make the unstable dynamics less regular in the resulting oscillation amplitudes.

There are several directions in which it would be relevant to extend the present considerations in the future. On the one hand, it would be relevant to generalize such binary states to "checkerboard" waveguide lattices in two-dimensional settings and to seek both the near continuum (as in [26, 28]) and the highly discrete limits of these and what can be said about the resulting nonlinear wave states. On the other hand, one could try to connect the states identified herein for small ε with the ones found in the above works for high ε. Naturally, only a few of the relevant configurations will persist all the way to the continuum limit of $\varepsilon \to \infty$, hence it would be useful to identify the bifurcations thereof and

how they may be similar or different (also depending on the specifics of C_1 and other parameters) from the standard DNLS case, explored e.g. in [31]. These topics are presently under study, and will be reported in future publications.

Acknowledgements. PGK gratefully acknowledges support from NSF-DMS-1312856, as well as from BSF-2010239 and from the ERC under FP7, Marie Curie Actions, People, International Research Staff Exchange Scheme (IRSES-605096). He also acknowledges the hospitality of the Center for Nonlinear Studies and the Los Alamos National Laboratory during the preparation of this work. Research at Los Alamos is supported in part by the US DoE. Work by ABA was supported by the National Science Foundation through the NSF-ECCS-1128593 IDR grant.

---

[1] S. Aubry, Physica **103D**, 201 (1997); S. Flach and C. R. Willis, Phys. Rep. **295**, 181 (1998); Physica **119D**, (1999), special volume edited by S. Flach and R. S. MacKay; focus issue edited by Yu. S. Kivshar and S. Flach, Chaos **13**, 586-799 (2003). S. Flach and A. V. Gorbach, Phys. Rep. **467**, 1 (2008).
[2] F. Lederer, G. I. Stegeman, D. N. Christodoulides, G. Assanto, M. Segev, and Y. Silberberg, Phys. Rep. **463**, 1 (2008).
[3] O. Morsch and M. Oberthaler, Rev. Mod. Phys. **78**, 179 (2006).
[4] M. Sato, B. E. Hubbard, and A. J. Sievers, Rev. Mod. Phys. **78**, 137 (2006).
[5] P. Binder, D. Abraimov, A. V. Ustinov, S. Flach, and Y. Zolotaryuk, Phys. Rev. Lett. **84**, 745 (2000); E. Trías, J. J. Mazo, and T. P. Orlando, Phys. Rev. Lett. **84**, 741 (2000).
[6] B. I. Swanson, J. A. Brozik, S. P. Love, G. F. Strouse, A. P. Shreve, A. R. Bishop, W.-Z. Wang, and M. I. Salkola, Phys. Rev. Lett. **82**, 3288 (1999).
[7] L. Q. English, M. Sato, and A. J. Sievers, Phys. Rev. B **67**, 024403 (2003); U. T. Schwarz, L. Q. English, and A. J. Sievers, Phys. Rev. Lett. **83**, 223 (1999).
[8] M. Peyrard, Nonlinearity **17**, R1 (2004).
[9] N. Boechler, G. Theocharis, S. Job, P. G. Kevrekidis, M. A. Porter, and C. Daraio, Phys. Rev. Lett. **104**, 244302 (2010).
[10] D. N. Christodoulides, F. Lederer, and Y. Silberberg, Nature **424**, 817 (2003); A. A. Sukhorukov, Y. S. Kivshar, H. S. Eisenberg, and Y. Silberberg, IEEE J. Quant. Elect. **39**, 31 (2003).
[11] H. S. Eisenberg, Y. Silberberg, R. Morandotti, A. R. Boyd, and J. S. Aitchison Phys. Rev. Lett. **81**, 3383 (1998).
[12] H. S. Eisenberg, Y. Silberberg, R. Morandotti, and J. S. Aitchison Phys. Rev. Lett. **85**, 1863 (2000).
[13] R. Iwanow, D. A. May-Arrioja, D. N. Christodoulides, G. I. Stegeman, Y. Min, and W. Sohler, Phys. Rev. Lett. **95**, 053902 (2005).
[14] C. E. Rüter, K. G. Makris, R. El-Ganainy, D. N. Christodoulides, M. Segev, and D. Kip, Nature Phys. **6**, 192 (2010).
[15] R. Morandotti, U. Peschel, J. S. Aitchison, H. S. Eisenberg, and Y. Silberberg Phys. Rev. Lett. **83**, 2726 (1999); R. Morandotti, H. S. Eisenberg, Y. Silberberg, M. Sorel, and J. S. Aitchison Phys. Rev. Lett. **86**, 3296 (2001).
[16] D. N. Neshev, T. J. Alexander, E. A. Ostrovskaya, Yu. S. Kivshar, H. Martin, I. Makasyuk, and Z. Chen, Phys. Rev. Lett. **92**, 123903 (2004).
[17] J. W. Fleischer, G. Bartal, O. Cohen, O. Manela, M. Segev, J. Hudock, and D. N. Christodoulides, Phys. Rev. Lett. **92**, 123904 (2004).
[18] V.A. Brazhnyi and V.V. Konotop, Mod. Phys. Lett. B **18**, 627 (2004).
[19] P. G. Kevrekidis, *The Discrete Nonlinear Schrödinger Equation*, Springer-Verlag (Heidelberg, 2009).
[20] J. Meier, J. Hudock, D. Christodoulides, G. Stegeman, Y. Silberberg, R. Morandotti, and J.S. Aithcison, Phys. Rev. Lett. **91**, 143907 (2003).
[21] R. L. Horne, P. G. Kevrekidis, and N. Whitaker, Phys. Rev. E **73**, 066601 (2006).
[22] R. Iwanow, R. Schiek, G. I. Stegeman, T. Pertsch, F. Lederer, Y. Min, and W. Sohler, Phys. Rev. Lett. **93**, 113902 (2004).
[23] H. Susanto, R. L. Horne, N. Whitaker, and P. G. Kevrekidis Phys. Rev. A **77**, 033805 (2008).
[24] E. Smirnov, C.E. Rüter, M. Stepić, D. Kip and V. Shandarov, Phys. Rev. E **74**, 065601 (2006).
[25] E. P. Fitrakis, P. G. Kevrekidis, H. Susanto, and D. J. Frantzeskakis Phys. Rev. E **75**, 066608 (2007).
[26] M. Conforti, C. De Angelis, T.R. Akylas, Phys. Rev. A **83**, 043822 (2011).
[27] A. Kanshu, C.E. Rüter, D. Kip, J. Cuevas and P.G. Kevrekidis, Europ. Phys. J. D **66**, 182 (2012).
[28] Matteo Conforti, Costantino De Angelis, T. R. Akylas, and Alejandro B. Aceves, Modulational stability and gap solitons of gapless systems: Continuous versus discrete limits, Phys. Rev. A **85**, 063836 (2012)
[29] R.S. MacKay and S. Aubry, Nonlinearity **7**, 1623 (1994).
[30] D.E. Pelinovsky, P.G. Kevrekidis, D.J. Frantzeskakis, Stability of discrete solitons in nonlinear Schrödinger lattices, Phys. D, **212**, 1, (2005)
[31] G.L. Alfimov, V.A. Brazhnyi, and V.V. Konotop, On classification of intrinsic localized modes for the discrete nonlinear Schrödinger equation, Physica D 194 (2004) 127-150.